species.[35] The details of the kinetic energy distributions were found to vary only weakly with structure or vibrational frequencies over the entire physically reasonable range for these quantities. The distributions were strongly dependent on the total energy available to the dissociating complex and hence in our model to the $\Delta H°$ of reaction.

(35) (a) Shimanouchi, T. *Table of Molecular Vibrational Frequencies*; National Bureau of Standards: Washington, DC, 1972; Consolidated, Vol. I. (b) Sverdlov, L. M.; Kovner, M. A.; Krainov, E. P. *Vibrational Spectra of Polyatomic Molecules*; Wiley: New York, 1970.

Often all heats of formation of products and reactants were well-known except one, the organometallic product ion. The heats of formation for Co(propene)$^+$ and Co(ethylene)$^+$ have been previously determined.[16b] The bond energies for the corresponding iron species as well as cobalta- and ferracyclobutane have also been determined.[17] These heats of formation were consistently used throughout the calculations and are summarized in Table II. All the parameters, except those for cyclopentane, have been previously published.[17] The parameters for cyclopentane are summarized in Table III.

# Electron-Transfer-Catalyzed Chelation of $[Fe(\eta^5\text{-}C_5R_5)(\eta^1\text{-}SC(S)NMe_2)(CO)_2]$ (R = H, Me) Induced by Oxidation

Jean-Noël Verpeaux,[†] Marie-Hélène Desbois,[‡] Alex Madonik,[§] Christian Amatore,*[,†] and Didier Astruc*[,‡]

*Laboratoire de Chimie, UA CNRS No. 1110, Ecole Normale Supérieure, 24 rue Lhomond, 75231 Paris Cédex 05, France, Laboratoire de Chimie Organique et Organométallique, UA CNRS No. 35, Université de Bordeaux I, 351, Cours de la Libération, 33405 Talence Cédex, France, and Laboratoire de Chimie des Organométalliques, UA CNRS No. 415, Université de Rennes I, 35042 Rennes Cédex, France*

*Received April 28, 1989*

The chelation of the monodentate dithiocarbamate complexes $[Fe(\eta^5\text{-}C_5R_5)(\eta^1\text{-dtc})(CO)_2]$ (dtc = SC(S)NMe$_2$; R = H (**1a**), Me (**1b**)) to $[Fe(\eta^5\text{-}C_5R_5)(\eta^2\text{-dtc})(CO)]$ (R = H (**2a**), Me (**2b**)) is catalyzed by $[FeCp_2]^+X^-$ ($X^-$ = $PF_6^-$ (**3a**), $BF_4^-$ (**3b**), $SbCl_6^-$ (**3c**)) in THF. The yields depend on the amount of **3** and on the size of its counteranion. The mechanism involves the oxidation $\mathbf{1} + \mathbf{3} \rightarrow \mathbf{2}^+X^- + FeCp_2$ and the cross electron transfer (ET) $\mathbf{2}^+X^- + \mathbf{1} \rightarrow \mathbf{2} + \mathbf{1}^+X^-$. However, the large endergonicity of the latter (>10 kcal mol$^{-1}$) makes it slow and side-reaction process(es) of $\mathbf{2}^+X^-$ (decomposition or precipitation) compete(s) efficiently with the cross-ET step. Accordingly the ETC mechanism proceeds eith low Coulombic efficiency (<5). Cyclic voltammetry (CV) does not allow the observation of $\mathbf{1}^+X^-$ even at scan rates $\simeq$5000 V s$^{-1}$, indicating that the chemical propagation step $\mathbf{1b}^+X^- \rightarrow \mathbf{2b}^+X^-$ proceeds at rate constants of ca. $10^7$ s$^{-1}$. It shows that the deactivating step of $\mathbf{2b}^+X^-$ proceeds with a rate constant of ca. $10^{-1}$ s$^{-1}$. CV's, in the presence of $PPh_3$, show the existence of $[FeCp^*(\eta^2\text{-dtc})(PPh_3)]^{+/0}$ ($\mathbf{4b}^+X^-/\mathbf{4b}$), and electrolysis of **1b** in the presence of electrolyte gives a THF-soluble one-electron-oxidation complex, presumably $[FeCp^*(\eta^2\text{-dtc})(THF)]^+X^-$ ($\mathbf{5b}^+X^-$).

## Introduction

There has been considerable interest, during this decade, in electron-transfer-chain (ETC) catalyzed organometallic reactions, i.e. reactions of organometallic complexes catalyzed by electrons or electron holes.[1-3] The principle of reactions catalyzed by electrons was pioneered by Kornblum[4] and Russell[5] in organic chemistry a quarter of a century ago, the most well-known series being Bunnett's $S_{RN}1$ reactions.[6] Using electrochemical techniques, Feldberg[7] established the theoretical and experimental basis for this electrocatalytic $\bar{E}C\bar{E}$ mechanism in 1971 at the same time as he disclosed the first example of a ligand-exchange reaction in organometallic chemistry. The dimensionless analysis of electrochemical kinetics by Savéant's group[8] was furthermore of considerable importance for the studies of, inter alia, the $\bar{E}C\bar{E}$ mechanism, particularly in the field of $S_{RN}1$ and related mechanisms.

Almost all the examples reported so far with the ETC mechanism have an exergonic cross-ET propagation step and, thus, are fast and complete.[8c] However, as already shown in $S_{RN}1$ reactions by Savéant's group, side reactions, a key problem in ETC catalysis, become especially im-

[†] Ecole Normale Supérieure.
[‡] Université de Bordeaux I.
[§] Université de Rennes I.

(1) Chanon, M. *Bull. Soc. Chim. Fr.* **1985**, 209; *Acc. Chem. Res.* **1987**, *20*, 214, and references cited in these reviews.
(2) Kochi, J. K. *J. Organomet. Chem.* **1986**, *300*, 139, and references cited in this review.
(3) Astruc, D. *Angew. Chem., Int. Ed. Engl.* **1988**, *27*, 643, and references cited in this review.
(4) (a) Kornblum, N.; Michel, R. E.; Kerber, R. C. *J. Am. Chem. Soc.* **1966**, *88*, 5662. (b) Kornblum, N. *Angew. Chem., Int. Ed. Engl.* **1975**, *14*, 734.
(5) (a) Russell, G. A.; Danen, W. C. *J. Am. Chem. Soc.* **1966**, *88*, 5563. (b) Russell, G. A. *Spec. Publ. Chem. Soc.* **1970**, *24*, 271.
(6) Bunnett, J. F. *Acc. Chem. Res.* **1978**, *11*, 413.
(7) Feldberg, S. W.; Jeftic, L. *J. Phys. Chem.* **1972**, *76*, 2439.
(8) (a) Savéant, J.-M. *Acc. Chem. Res.* **1980**, *13*, 323. (b) Amatore, C.; Savéant, J.-M. *J. Electroanal. Chem. Interfacial Electrochem.* **1983**, *144*, 59. (c) Amatore, C.; Pinson, J.; Savéant, J.-M.; Thiébault, A. *J. Electroanal. Chem. Interfacial Electrochem.* **1980**, *107*, 59, 75. (d) Zizelman, P. M.; Amatore, C.; Kochi, J. K. *J. Am. Chem. Soc.* **1984**, *106*, 3721.

0276-7333/90/2309-0630$02.50/0 

Chart I

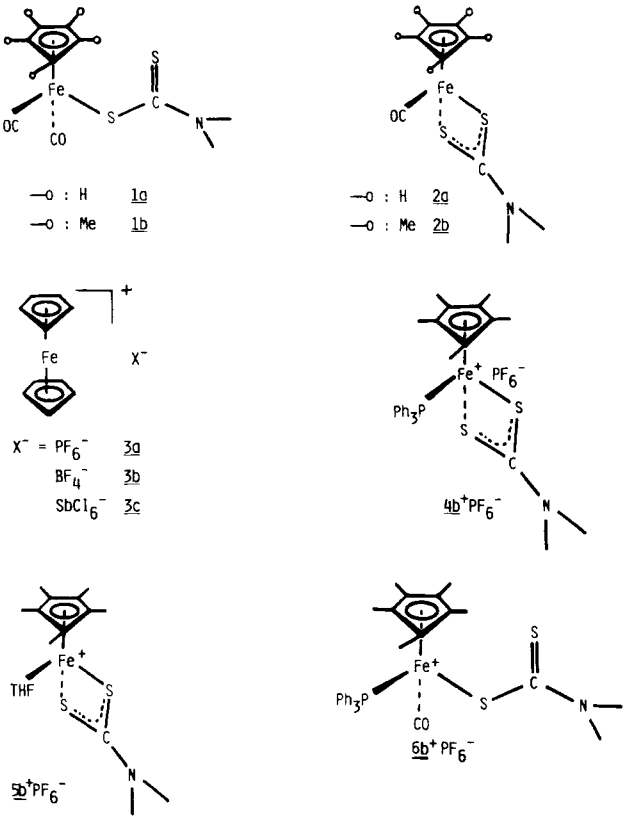


portant when the cross-ET propagation step is endergonic.[9] Indeed, the numerous reports of ligand-exchange reactions on mononuclear complexes involve oxidative induction of the replacement of a ligand by a less electron-releasing one. The reverse is true in cluster chemistry, where carbonyls are replaced by more electron-releasing P donors by reductive initiation. All these reactions have an exergonic ET propagation step.

The present case, one of the first studies of the chelation of a ligand,[9,10] is indeed a special example of ligand exchange since the chelation of the dithiocarbamate ligand is accompanied by removal of a CO ligand. In contrast with most of the other known examples of ligand exchanges in mononuclear complexes, the present one thus involves replacement of CO by a *more* electron-releasing sulfur ligand.[11] Besides its originality, this may result in a difficulty in the very mechanism of ETC. Indeed, the latter implies a cross electron transfer between the oxidized form of the resulting product and the neutral one of the reactant, as indicated by the last reaction of the propagating sequence. According to the Marcus theory[12] the cross-ET propagation step should now be slow but the driving force is provided by the chemical propagation step (chelation). Yields and Coulombic efficiencies are thus relatively low, which allow an easier study of factors such as the medium of the ETC-catalyzed reaction. After a preliminary communication,[10] we detail here the electrochemical and ET studies, the role of the counteranion of the initiator ferrocenium, and the mechanistic consequences of these findings.

Table I. Influence of the Quantity of Catalyst on the Evolution of Chelation of Complex 1b

| % of added $[FeCp_2]^+$-$PF_6^-$ | % of unreacted 1b[a] | % of 2b formed[a] | catalytic activity[b] | % of $2b^+PF_6^-$ formed[a] |
|---|---|---|---|---|
| 5 | 67 | 20 | 4.0 | 4 |
| 7 | 60 | 31 | 4.4 | 6 |
| 10 | 54 | 36 | 3.6 | 7 |
| 15 | 38 | 45 | 3.0 | 11 |
| 20 | 33 | 41 | 2.0 | 19 |
| 30 | 27 | 33 | 1.1 | 30 |
| 40 | 22 | 31 | 0.8 | 39 |
| 50 | 7 | 33 | 0.7 | 49 |
| 100 | 0 | 0 | 0.0 | 95 |

[a] All the reactions were worked up on a 0.5 mM scale, and all the yields are given for isolated complexes. [b] The catalytic activity is given by the ratio between the quantities of complex **2b** formed and that of the added catalyst.

## Results

**I. Heat- and Light-Induced Chelation.** The known dithiocarbamate complexes $[Fe(\eta^5\text{-}C_5R_5)(\eta^1\text{-dtc})(CO)_2]$ (dtc = $SC(S)NMe_2$; **1a** (R = H)[13] and **1b** (R = Me)[14]) can be heated to give the chelates $[Fe(\eta^5\text{-}C_5R_5)(\eta^2\text{-dtc})(CO)]$ (**2a** (R = H) and **2b** (R = Me)) in very low yields as already reported (Chart I). The reactions proceed along with considerable decomposition. At 20 °C, the noncatalyzed process is inefficient.[13a]

On the other hand, the photolysis of **1** by visible light is a very efficient process, giving **2** cleanly. Exposure of a millimolar solution of **1b** to sunlight for 2 h or to a 150-W visible lamp for 1 h gave a complete conversion to **2b**. The mechanism of the photoreaction is detailed in the following article (eq 1).

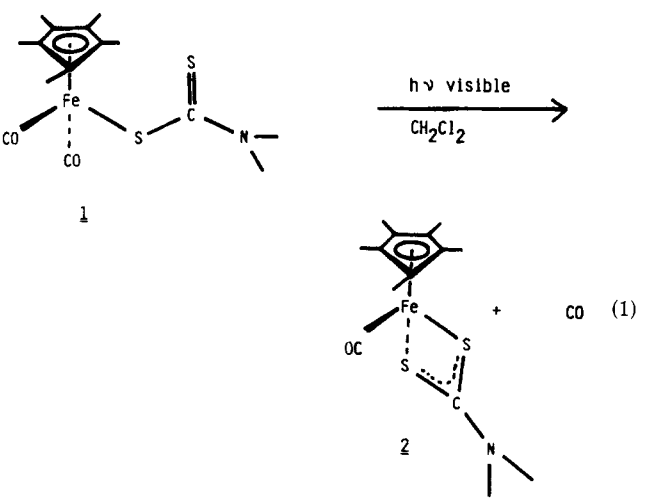


**II. Chelation Induced by Ferrocenium Salts.** The reaction **1** → **2**, induced by $[FeCp_2]^+[PF_6]^-$ (**3a**)[15] in THF, was monitored by infrared and $^1H$ NMR spectroscopies (eq 2). The relative intensities of the carbonyl bands (2040

(9) (a) Catheline, D.; Astruc, D. *Int. Conf. Coord. Chem.* **1982**, *23*, Fr 41. (b) Astruc, D. *Acc. Chem. Res.* **1986**, *19*, 377. (c) Moran, M.; Cuadrado, J.; Masaguer, J. R.; Losada, J. *J. Organomet. Chem.* **1987**, *335*, 255. (d) Moran, M.; Cuadrado, J.; Masaguer, J. R.; Losada, J. *J. Chem. Soc., Dalton Trans.* **1988**, 149.

(10) Amatore, C.; Verpeaux, J.-N.; Madonik, A. M.; Desbois, M.-H.; Astruc, D. *J. Chem. Soc., Chem. Commun.* **1988**, 200.

(11) For exchange of CO by a more electron-releasing ligand in mononuclear complexes occurring by electrocatalysis, see: Lahuerta, P.; Latorre, J.; Sanau, M. *J. Organomet. Chem.* **1986**, *286*, C27.

(12) (a) Marcus, R. A. *Discuss. Faraday Soc.* **1960**, *29*, 21. (b) Marcus, R. A. *Can. J. Chem.* **1959**, *37*, 155. (c) Marcus, R. A. *J. Phys. Chem.* **1963**, *67*, 853.

(13) (a) O'Connor, C. O.; Gilbert, J. D.; Wilkinson, G. *J. Chem. Soc. A* **1969**, 84. (b) Abel, A. W.; Dunster, M. O. *J. Chem. Soc., Dalton Trans.* **1973**, 58. (c) Román, E.; Catheline, D.; Astruc, D. *J. Organomet. Chem.* **1982**, *236*, 229.

(14) (a) Catheline, D.; Román, E.; Astruc, D. *Inorg. Chem.* **1984**, *23*, 4508. (b) Catheline, D.; Astruc, D. *J. Organomet. Chem.* **1984**, *266*, C11.

(15) For a recent preparation, see: Desbois, M.-H.; Astruc, D. *New. J. Chem.* **1989**, *13*, 585.

$$1 \xrightarrow{[FeCp_2]^+[PF_6]^-} 2 + CO \qquad (2)$$

(s) $cm^{-1}$ for **1a** and 1940 (s) $cm^{-1}$ for **2a**, 2000 (s) $cm^{-1}$ for **1b** and 1910 (s) $cm^{-1}$ for **2b**)[16] gave a semiquantitative measure of the progress of the reaction (the reactant and product have roughly the same extinction coefficient). No change occurred in the infrared spectra after a few minutes at 20 °C. Titration using $^1H$ NMR spectroscopy also gave concordant results.

Table I indicates the yields of **2b** and **2b**$^+$ formed and unreacted **1b** for various amounts of **3a** (0.05–1 equiv). The maximum yield is obtained for 0.15 equiv of **3a**, reaching 45%, and the best Coulombic efficiency is only 4.4 for 0.07 equiv of **3a**. Complex **3a** is not soluble at the start of the reaction but is progressively solubilized as it is transformed (quantitatively) to ferrocene.

As the reaction goes on, a complex precipitates, whereas the chelate **2a** (or **2b**) remains in solution. In the case of the chelation of **1b**, this THF-insoluble complex is stable and is identified as the 17e complex $[Fe^{III}Cp^*(\eta^2\text{-dtc})(CO)]^+[PF_6]^-$ (**2b**$^+PF_6^-$).[16] There is no decomposition in the reactions of **1b** with various amounts of **3a**. Some unreacted complex **1b** is always found up to 0.5 equiv of **3a**, and the final ratio of the reaction shows that converted **1b** only gives **2b** and **2b**$^+PF_6^-$. When the amount of **3a** is increased, the yield of **2b**$^+PF_6^-$ is increased and is proportional to that of added **3a**; it is quantitative for 1 equiv of **3a** (Table I and eq 3).

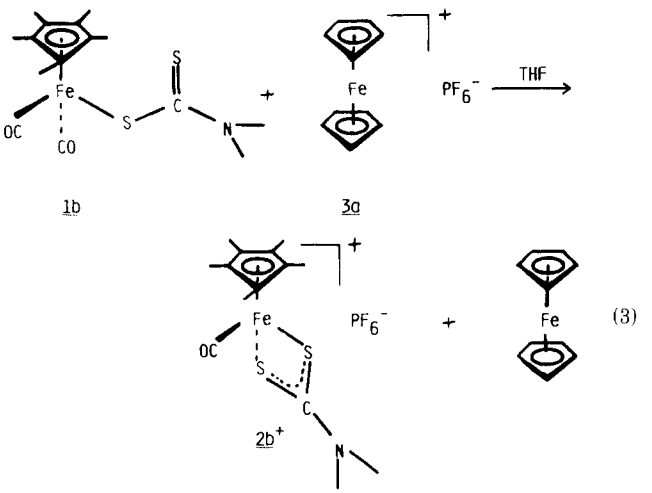


(3)

In the presence of 1 equiv of $PPh_3$, the stoichiometric oxidation in acetone gives the analogous 17e complex:

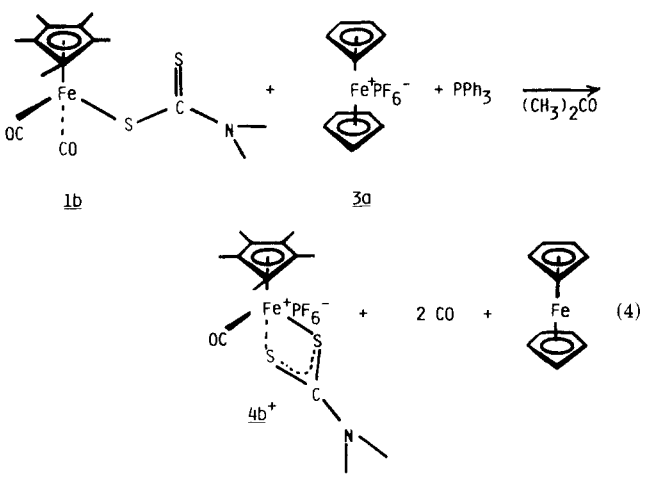


(4)

(16) Desbois, M.-H.; Astruc, D. *Angew. Chem., Int. Ed. Engl.* **1989**, *28*, 459.

**Table II. Influence of the Nature of the Counteranion of the Catalyst on the Yields of the Reaction of Chelation: $[Fe(\eta^5\text{-}C_5R_5)(\eta^1\text{-dtc})(CO)_2]$ + 10% $[FeCp_2]^+X^-$ → $[Fe(\eta^5\text{-}C_5R_5)(\eta^2\text{-dtc})(CO)]$ (R = H or Me)**

| $X^-$ | % in **2a** | % in **2b** |
|---|---|---|
| $BF_4^-$ | 47 | 23 |
| $PF_6^-$ | 52 | 36 |
| $SbCl_6^-$ | 63 | 38 |

These studies show that ferrocenium plays the role of a catalytic electron hole (Table I). However, the THF-insoluble complex **2b**$^+PF_6^-$ does not react with **1b** in the catalytic reactions as suggested in eq 5. Thus, the pre-

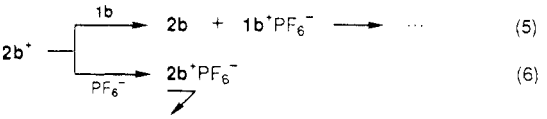


cipitation of **2b**$^+PF_6^-$ is critical since **2b**$^+PF_6^-$ should react with **1b** to close the propagation cycle. This reaction of **2b**$^+PF_6^-$ with **1b** must occur before precipitation. Thus, the precipitation of **2b**$^+PF_6^-$ (eq 6) is a side-reaction process inhibiting the propagation of the chain, especially because the cross-ET step is endergonic and therefore slow. In the case of **1a**, the results are similar but **2a**$^+PF_6^-$ decomposes, which also breaks the propagation cycle.

Since the rate of precipitation is high in the context of a slow, endergonic cross-ET step, it appeared timely to investigate the role of the counteranion of ferrocenium on the ETC catalysis. Thus, we effected a series of catalytic chelation reactions using various ferrocenium salts ($PF_6^-$, **3a**; $BF_4^-$, **3b**; $SbCl_6^-$, **3c**). The yields and conversion rates are indicated in Table II for both Cp and Cp* series. They clearly show the influence of the counteranion on the reaction yield. The yields are higher as the counteranion becomes larger in both Cp and Cp* series; the conversion remains high. This indicates that the precipitation of $2^+$ is slower when the counteranion is larger. The mechanism of the ETC catalysis of chelation is summarized in Scheme I.

We have also investigated the electrocatalytic chelation in dichloromethane in which no precipitation occurs. The yield of **2b** obtained from **1b** with use of 0.1 equiv of $[FeCp_2]^+[PF_6]^-$ is only 12%, while most of **1b** is recovered. We know[16] that **2b**$^+$ reacts with $CH_2Cl_2$ according to

$$2b^+PF_6^- + CH_2Cl_2 \rightarrow [FeCp^*(\eta^2\text{-dtc})(CH_2Cl_2)]^+[PF_6]^- + CO$$

This CO substitution reaction disrupts the catalytic ET chain. The low yield obtained indicates that the cross-ET step is slower than side reactions of **2b**$^+PF_6^-$.

Another way to perform the electrocatalytic chelation under homogeneous conditions is to use $[nBu_4N]^+[BF_4]^-$ in THF. It was found subsequent to the coulometric experiment (vide infra) that $[nBu_4N]^+[BF_4]^-$ had the ability to solubilize $2^+BF_4^-$ in THF. Remarkably, the yields of the electrocatalytic chelation under these homogeneous conditions are rather close to those found when $2^+PF_6^-$ precipitates (absence of $[nBu_4N]^+[BF_4]^-$). This indicates that the rates of chain deactivation under homogeneous and heterogeneous conditions are of the same order of magnitude.

**III. Electrochemical Investigation of the ETC Catalysis of Ligand Substitution. A. Electrochemically Induced Chelation in $[FeCp^*(\eta^1\text{-dtc})(CO)_2]$ (1b).** The cyclic voltammetry of $[FeCp^*(\eta^1\text{-dtc})(CO)_2]$ (**1b**) in Figure 1 demonstrates the facile conversion of the cation radical **1b**$^+$, formed at the oxidation wave $O_1$, into the rather stable

**Scheme I**

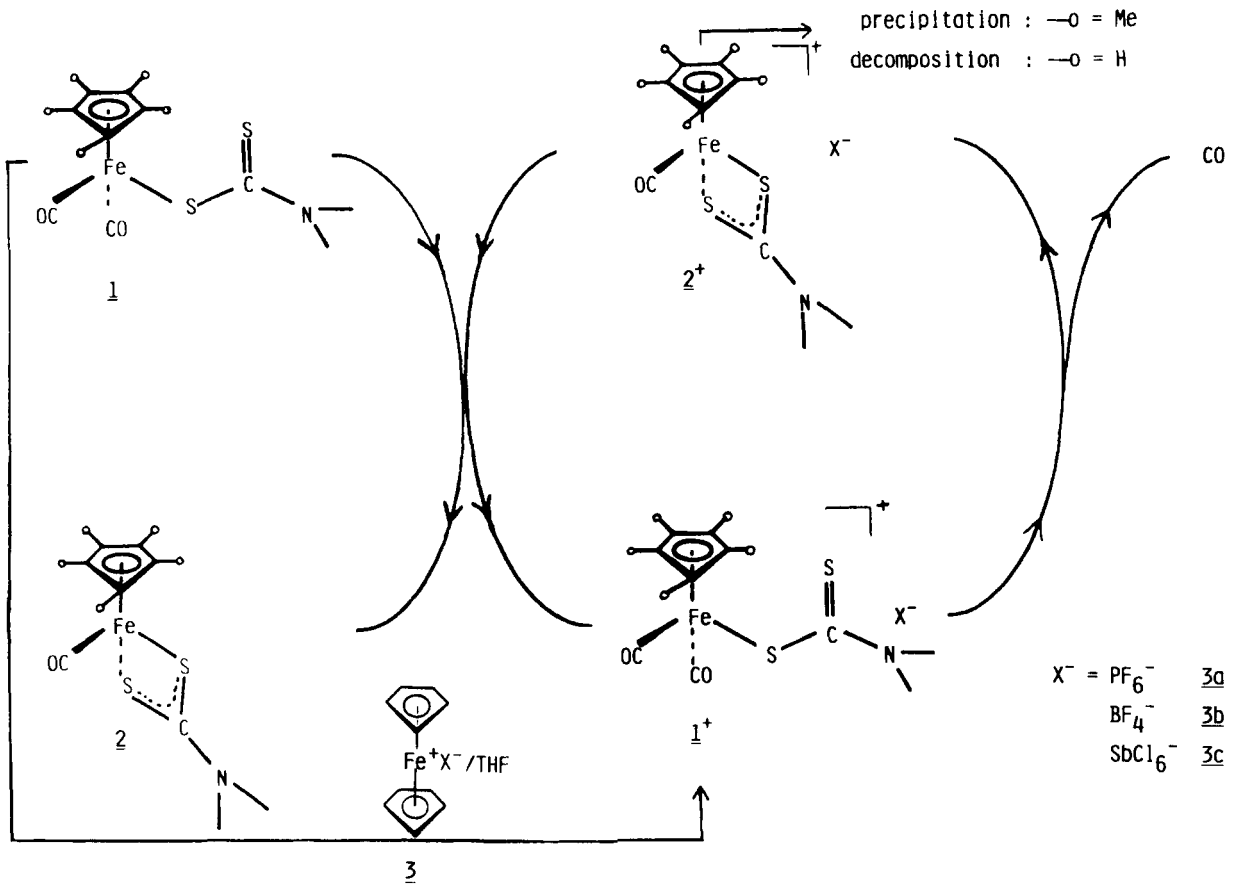


**Scheme II**

$$\mathbf{1b} \underset{+e^-}{\overset{-e^-}{\rightleftharpoons}} \mathbf{1b^+} \quad \text{oxidation wave } O_1 \qquad (7)$$

$$\mathbf{1b^+} \rightarrow \mathbf{2b^+} \qquad (8)$$

$$\mathbf{2b^+} \underset{-e^-}{\overset{+e^-}{\rightleftharpoons}} \mathbf{2b} \quad \text{reduction wave } R_2 \qquad (9)$$

**Scheme III**

$$\mathbf{1b} + \mathbf{2b^+} \underset{k_{-10}}{\overset{k_{10}}{\rightleftharpoons}} \mathbf{1b^+} + \mathbf{2b} \qquad (10)$$

$$\mathbf{1b^+} \xrightarrow{k_{11}} \mathbf{2b^+} \qquad (11)$$

cation radical [FeCp*($\eta^2$-dtc)(CO)]$^+$ (**2b**$^+$), which is further reduced upon scan reversal at wave $R_2$, as summarized in Scheme II, leading to the overall conversion of the monodentate (dimethyldithiocarbamato)iron(III) dicarbonyl to the chelated (dimethyldithiocarbamato)iron(II) derivative.

However, within the time scale of the cyclic voltammetry in Figures 1 and 2 the process is not electrocatalytic since **2b**$^+$ is not reducible at the potential location where the oxidation wave $O_1$ is observed. Indeed, continuous cycling of the potential over the potential location of the $R_2/O_2$ wave in Figure 2 shows that almost no conversion of the monodentate complex into the bidentate one is observed unless the anodic limit of the scan is increased to reach the foot of the wave $O_1$. Yet, in this respect, it is of importance to note that a scan rate of 20 V s$^{-1}$, used for the cyclic voltammetries in Figures 1 and 2, corresponds to a millisecond time scale. Indeed, when a slower time scale

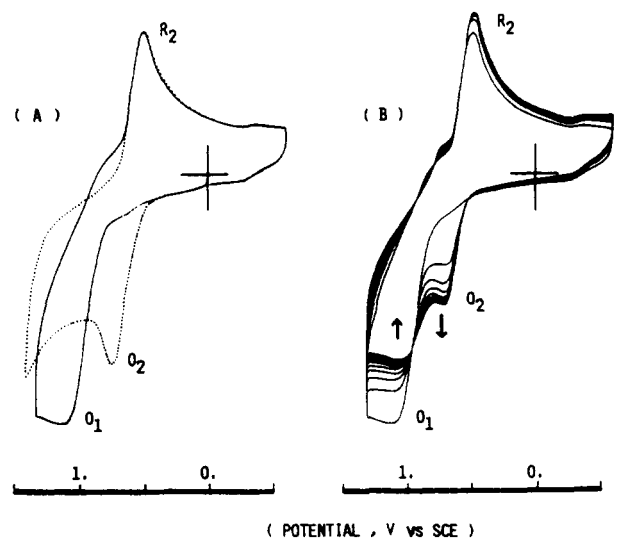


**Figure 1.** CV of a 2 mM solution of **1b** in THF with 0.3 M [$n$Bu$_4$N$^+$][BF$_4^-$] at a scan rate of 20 V s$^{-1}$. (A) Single-scan CV. (B) Repetitive-scan CV, showing the appearance of complex FeCp*($\eta^2$-dtc)(CO), **2b** ($O_2/R_2$), concomitant with the disappearance of complex FeCp*($\eta^1$-dtc)(CO)$_2$, **1b** ($O_1$). The CV of an authentic sample of **2b** under identical conditions is shown as a broken line in A. Potentials refer to the standard calomel reference electrode.

is considered ($\delta < 1$ V s$^{-1}$, i.e. $\theta > 25$ ms) as in Figure 3, it is seen that the oxidation wave $O_2$ increases with respect to $O_1$ when the scan rate is decreased. This phenomenon originates from the facile electrocatalytic process in Scheme III under electrochemical stimulation at the potential of wave $O_2$.[8c]

Indeed, the uphill electron transfer (eq 10) can be continuously displaced by the irreversible intramolecular

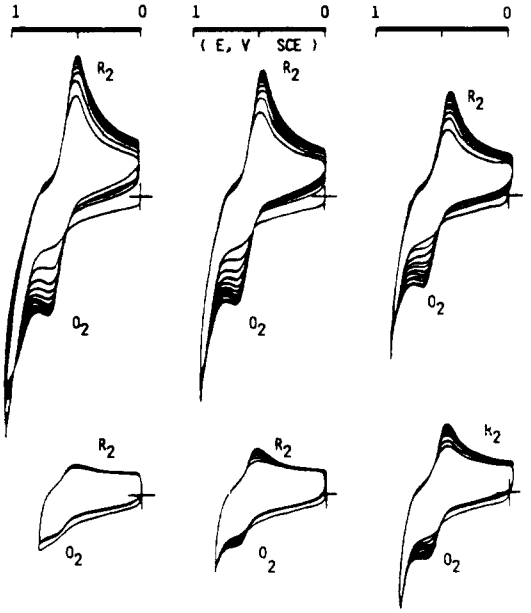


**Figure 2.** CV of a 2 mM solution of **1b** in THF with 0.3 M $[nBu_4N^+][BF_4^-]$. Effect of the inversion potential on the chain propagation in repetitive scan CV (20 V $s^{-1}$).

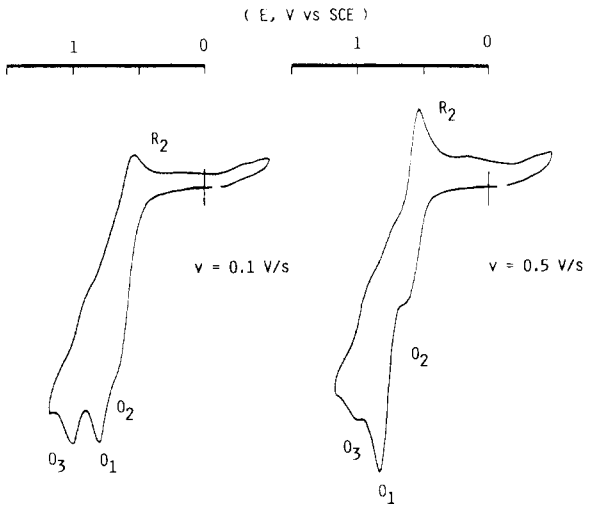


**Figure 3.** CV of a 2 mM solution of **1b** in THF with 0.3 M $[nBu_4N^+][BF_4^-]$ at 0.1 and 0.5 V $s^{-1}$.

ligand substitution in eq 11. This sequence is tantamount to the overall conversion of **1b** into **2b** and proceeds with a half-life time that can be estimated at approximately 1 s, from the data in Figure 3. However, a precise determination is not easy, owing to the explosive chain character of the mechanism in reactions (eqs 10 and 11) when the electrode potential is set on the $O_2$ wave. Indeed, under such conditions **2b** formed in eq 10 is oxidized at the electrode, the overall sequence then becoming autocatalytic:[8c]

$$\mathbf{1b} + \mathbf{2b}^+ \rightarrow 2\ \mathbf{2b}^+ + e^- + CO \qquad (12)$$

Moreover, the efficiency of the process in Scheme III is established by the fact that the recording of several voltammograms, in the dark, was enough to convert ca. 25% of **1b** into **2b** within 2 h under the conditions of Figure 1 (compare to a half-life of ca. 50 h under the same conditions without electrochemical stimulation of the chain).

**B. Cyclic Voltammetry of the Complexes FeCp*($\eta^2$-dtc)(CO) (2b) and $[FeCp^*(\eta^2\text{-dtc})(PPh_3)]^+[PF_6]^-$ ($\mathbf{4b^+PF_6^-}$).** The oxidative cyclic voltammograms, presented in Figure 4, correspond to the one-electron uptake

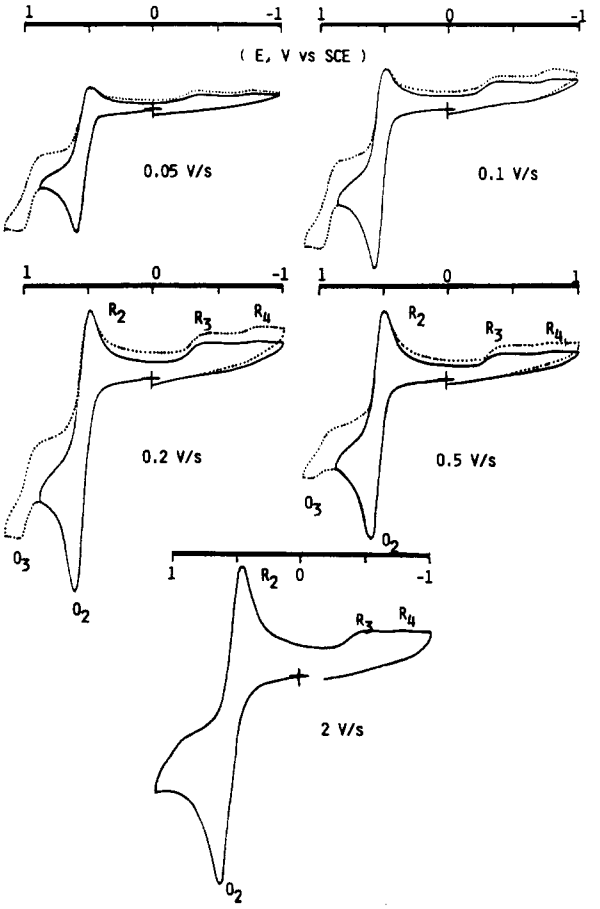


**Figure 4.** CV's of a 2 mM solution of **2b** in THF with 0.3 M $[nBu_4N^+][BF_4^-]$, at different scan rate showing the evolution of the cationic species $\mathbf{2b^+}$.

from **2b** (wave $O_2$) to afford the cation radical $\mathbf{2b^+}$. Under the experimental conditions used, the latter is chemically stable on the millisecond time scale as shown by the chemical reversibility of the $O_2/R_2$ voltammogram at high scan rates ($v > 10$ V $s^{-1}$; Figure 1A). At lower scan rates the wave $R_2$, featuring $\mathbf{2b^+}$ reduction to the starting iron complex, decays, showing that, in this context, the cation radical chemically evolves before it can be reduced as in eq 13. No direct evidence of the nature of the chemistry involved can be obtained from the voltammograms in Figure 4.

$$\mathbf{2b} \underset{+e^-}{\overset{-e^-}{\rightleftharpoons}} \mathbf{2b^+} \rightarrow \ldots \qquad (13)$$

However, the decay of the peak current of wave $R_2$ is concomitant with the growth of a set of three additional waves, $R_3$, $R_4$, and $O_3$, which are then attributed respectively to the reduction and oxidation of product(s) from the chemical evolution of $\mathbf{2b^+}$. The relative heights of waves $O_3$ and $R_3$ are independent of the scan rate, suggesting that they are related to the same species. In contrast, wave $R_4$ depends on the scan rate and the potential scan extent, which indicates that the product reduced at $R_4$ is formed along a competitive pathway or rather results from further evolution.[17]

(17) (a) Nadjo, A. J.; Savéant, J.-M. *J. Electroanal. Chem.* **1973**, *48*, 113. (b) Bard, A. J.; Faulkner, L. R. In *Electrochemical Methods*; Wiley: New York, 1980. (c) Andrieux, C. P.; Savéant, J.-M. In *Investigation of Rates and Mechanisms*; Bernasconi, C. F., Ed.; Wiley: New York, 1986; Vol. 6, 4/E, Part 2, pp 305–390.

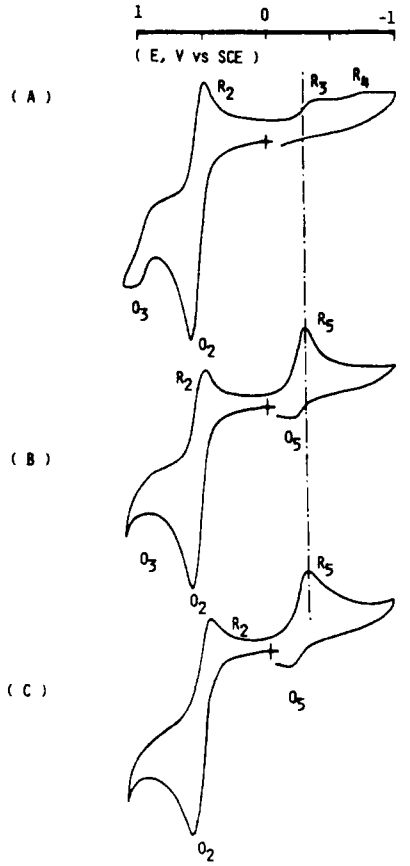


**Figure 5.** CV's of a 2 mM solution of **2b** in THF with 0.3 M $[nBu_4N^+][BF_4^-]$, at 0.1 V $s^{-1}$ in the presence of 0 (A), 1 (B), and 3 equiv (C) of triphenylphosphine.

Figure 5 shows that wave $O_2/R_2$ is not affected, either in potential location or in shape and percent of reversibility, by the presence of stoichiometric amounts of added triphenylphosphine. This is clear evidence that within the time scale of cyclic voltammetry the cation **2b**$^+$ formed at wave $O_2$ is chemically inert to triphenylphosphine. However, waves $O_3$, $R_3$, and $R_4$ then totally disappear while a new reduction wave, $R_5$, is observed. The latter, whose height is independent of the triphenylphosphine excess (1–3 equiv), features the reduction wave of the phosphine-substituted bidentate (dimethyldithiocarbamato)-iron(III) cyclopentadienyl cation **4b**$^+PF_6^-$ as established by comparison with that of an authentic sample (vide infra and Figure 6).

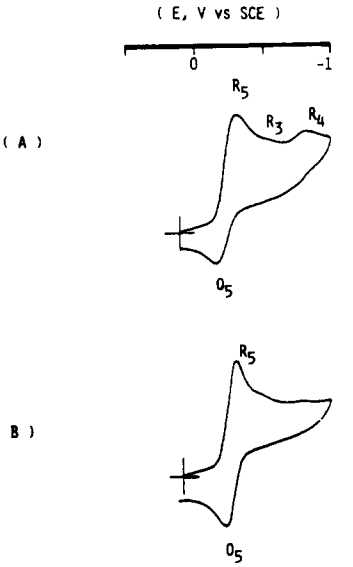


**Figure 6.** CV's of a 2 mM solution of $[FeCp^*(\eta^2\text{-dtc})(PPh_3)]^+PF_6^-$ in THF with 0.3 M $[nBu_4N^+][BF_4^-]$ in the presence of 0 (A) and 1.2 equiv (B) of $PPh_3$.

The reduction voltammogram of **4b**$^+PF_6^-$, shown in Figure 6, indicates that the neutral complex **4b**, formed through a one-electron intake at $R_5$, is only partially stable under these conditions. Indeed, the oxidation current at wave $O_5$, observed after scan reversal, shows that only ca. 50% of **4b** is reoxidized back to **4b**$^+PF_6^-$ at $v = 0.5$ V $s^{-1}$ ($\theta = 50$ ms):

$$\mathbf{4b}^+PF_6^- + e^- \rightarrow \mathbf{4b} \rightarrow \ldots \quad (14)$$

This loss of reversibility corresponds to the appearance of two reduction waves identical with those of $R_3$ and $R_4$, observed during the cyclic voltammetry of **2b** (vide supra and Figure 5). In the presence of added triphenylphosphine, the latter waves disappear while the reversibility of wave $R_5/O_5$ is restored (compare parts A and B of Figure 6). Such a behavior indicates that the chemical reaction in eq 14 involves reversible phosphine expulsion as the first step in eq 15.

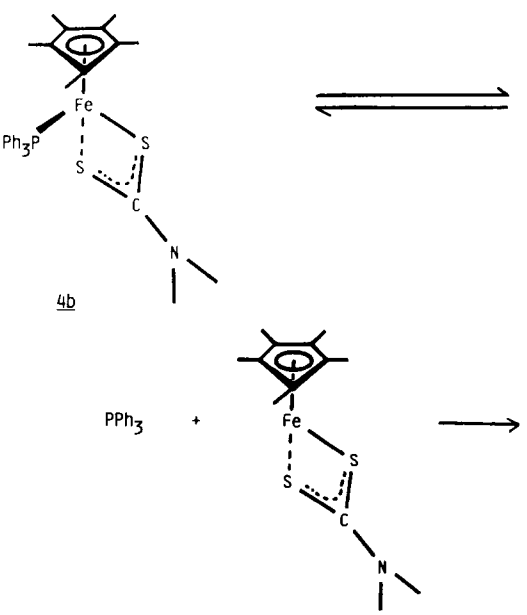


(15)

**C. Coulometry.** Electrolysis of 1 mmol of **1b** in THF containing $[nBu_4N]^+[BF_4]^-$ (0.3 M) at +1.0 V vs SCE (after preelectrolysis) on Pt gauze as the anode leads to the

(18) The equilibrium constant $K_{10} = k_{10}/k_{-10}$ corresponds to the homogeneous electron transfer in eq 10. Thus if $O_1$ is for oxidation wave of complex 1), $K_{10} = \exp[F(E^\circ_{O_2} - E^\circ_{O_1})/RT]$. Wave $O_2$ being quasi-reversible, $E^\circ_{O_2}$ can be approximated within a reasonable accuracy (±10 mV) by $(E^p_{O_2} + E^p_{R_2})/2$.[17] Wave $O_1$ is chemically irreversible but is not controlled by the kinetics of the electron transfer provided $v < 10$ V $s^{-1}$. A precise determination of the kinetic control of the wave is made difficult since at low scan rates ($v < 1$ V $s^{-1}$) the propagation of the electrocatalytic chain interfers.[8c] As a result in the intermediate range ($1 \leq v \leq 10$ V $s^{-1}$) where the wave is mainly controlled by the follow-up chemical step (eq 11), a continuous variation of $E^p_{O_1}/\log v$ is observed with an average value 30 mV, rather than a straight line.[17] In this range of scan rates the peak potential of wave $O_1$ can thus be estimated by[17a]

$$E^p_{O_1} = E^\circ_{O_1} + 0.78(RT/F) - (RT/2F) \ln (k_{11}RT/Fv)$$

Introduction of this equation in the definition of $K_{10}$ yields

$$K_{10}(k_{11})^{1/2} = \exp[F(E^\circ_{O_2} - E^p_{O_1})/RT + 0.78]/(RT/Fv)^{1/2}$$

The validity of this equation was verified by the constancy, within the accuracy of the measurements, of the product $K_{10}(k_{11})^{1/2}$ as a function of the scan rate in the range $1 < v < 10$ V $s^{-1}$. Thus an average value $K_{10}(k_{11})^{1/2} \simeq 2 \times 10^{-4}$ was obtained.

consumption of 1 faraday/mol of **1b**. A brown homogeneous THF solution evolved from the oxidation. Notably a cathodic reduction cyclic voltammogram performed on the solution obtained after electrolysis showed the presence of the set of two reduction waves $R_3$ and $R_4$, in agreement with the results of microscale electrolysis in Figure 4 or 5A. The corresponding thermally stable organometallic complex was not separated from the electrolyte but was identified by its ESR and infrared spectra being identical with those of an authentic sample of $[FeCp^*(\eta^2\text{-dtc})(THF)]^+[BF_4]^-$ ($\mathbf{5b}^+BF_4^-$)[16] (absence of CO band and presence of coordinated THF ones). Note that, in the absence of the electrolyte, the complexes $\mathbf{2b}^+BF_4^-$ and $\mathbf{2b}^+PF_6^-$ are stable because of their precipitation. This has been checked by using $[FeCp_2]^+[BF_4]^-$ as well as $[FeCp_2]^+[PF_6]^-$ as oxidants. We have also performed the oxidation with $[FeCp_2]^+[BF_4]^-$ in the presence of 3 equiv of $[nBu_4N]^+[BF_4]^-$ and observed that the CO exchange by THF was quantitatively found instead of the precipitation of $\mathbf{2b}^+BF_4^-$. The role of $[nBu_4N]^+[BF_4]^-$ consists of solubilizing $\mathbf{2b}^+BF_4^-$ by the well-known "salt-in" effect of its large organic cation:[19]

$$\underset{\mathbf{2b}^+BF_4^-}{[FeCp^*(\eta^2\text{-dtc})(CO)]^+[BF_4]^-} \xrightarrow[THF]{[nBu_4N]^+[BF_4]^-} \underset{\mathbf{5b}^+BF_4^-}{[FeCp^*(\eta^2\text{-dtc})(THF)]^+[BF_4]^-}$$

We also know that $\mathbf{2b}^+$ reacts rapidly in solution with THF to give a CO exchange with THF.[16] This was shown to be the case in a mixture of dichloromethane and THF in the absence of $[nBF_4N]^+[BF_4]^-$. In summary, both dichloromethane and $[nBu_4N]^+[BF_4]^-$ can solubilize $\mathbf{2b}^+X^-$ ($X^- = PF_6^-, BF_4^-$), the condition necessary for CO exchange by THF. In this reaction, the chelation of the dtc ligand consumes no net current flow and is followed by stoichiometric oxidation (1e) and ligand exchange ($\bar{E}C\bar{E}$ + $\bar{E}C$). This reaction is also completely analogous to the oxidation in the presence of $PPh_3$.

## Discussion

**I. Electron-Transfer Catalysis of 1b to 2b Conversion.** The cyclic voltammetry of $[FeCp^*(\eta^1\text{-dtc})(CO)_2]$ (**1b**) demonstrates the facile intramolecular ligand substitution of the carbon monoxide ligand to afford the bidentate (dimethyldithiocarbamato)iron complex **2b**. This process, which is formally noncatalytic under electrochemical conditions, **2b** being more easily oxidizable than **1b**, becomes catalytic owing to the propagating sequence in Scheme III. Indeed, the fast CO substitution by dtc chelation in eq 11, removing $\mathbf{1b}^+$, is sufficient to overcome the energetic barrier of at least 0.275 V in the uphill electron transfer (eq 10). Thus, the combined sequence of reactions eq 10 + eq 11, which amounts to the overall catalytic conversion of **1b** into **2b**, proceeds with the rate law in eq 16.

$$d[\mathbf{1b}]/dt = -k_{11}k_{10}[\mathbf{1b}][\mathbf{2b}^+]/(k_{11} + k_{-10}[\mathbf{2b}]) \quad (16)$$

Two limiting rate laws will be observed according to the respective importance (i) of the backward electron transfer in reaction 10 and (ii) of the overall intramolecular ligand substitution in reaction 11. When $k_{11} \gg k_{-10}[\mathbf{2b}]$, the electron transfer is kinetically irreversible, being then the rate-determining step: thus, eq 16 simplifies to kinetic eq 17.

**Scheme IV**

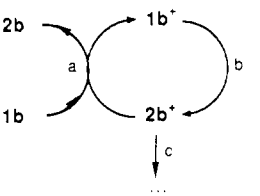


$$d[\mathbf{1b}]/dt \simeq -k_{10}[\mathbf{2b}^+][\mathbf{1b}] \quad (17)$$

The opposite occurs when $k_{11} \ll k_{-10}[\mathbf{2b}]$. The electron transfer acts as a rapid preequilibrium, the intramolecular ligand exchange being the rate-determining step:

$$d[\mathbf{1b}]/dt \simeq -(k_{11}k_{10}/k_{-10})[\mathbf{2b}^+][\mathbf{1b}]/[\mathbf{2b}] \quad (18)$$

Owing to the large endergonicity of the electron transfer in eq 10, $k_{-10}$ can be accurately estimated as being close to the diffusion limit rate constant, i.e., ca. $3 \times 10^9$ $M^{-1}$ $s^{-1}$. On the other hand, from the relative peak positions of the oxidation waves $O_1$ and $O_2$, one can estimate[18] the equilibrium constant $K_{10} = k_{10}/k_{-10}$ as being of the order of $2 \times 10^{-4}k_{11}^{-1/2}$, $k_{11}$ expressed in $s^{-1}$. Then it ensues that $k_{10} \simeq 6 \times 10^5 k_{11}^{-1/2}$ $M^{-1}$ $s^{-1}$. Thus, for the experimental conditions in Figure 3, the half-life of **1b**, for the electrode potential located at the rising branch of wave $O_2$, can be predicted as ca. $10^{-3}k_{11}^{1/2}$ s if the forward electron transfer is rate determining or ca. $3 \times 10^3 k_{11}^{-1/2}$ s if the rate-determining step (rds) is the ligand exchange. Thus, comparison with the experimental lifetime leads[17] to an estimate of $10^6$ or $10^7$ $s^{-1}$ for the rate constant $k_{11}$, according to each limiting situation, respectively. Such orders of magnitude of $k_{11}$ agree with the overall efficiency of the catalytic conversion in Scheme II and with the fact that no limit of reversibility has been observed for the oxidation wave of the monodentate dtc complex **1b** up to scan rates of 5000 V $s^{-1}$ (i.e., $k_{11} > 2 \times 10^6$ $s^{-1}$).[17] On the other hand, the relative identity, owing to the approximations involved in their determinations, of the two above figures indicates that the backward electron transfer and the ligand exchange have nearly identical rates in the experimental conditions considered here. Then, for the homogeneous experiments in Table I, the apparent rate of the overall conversion **1b** to **2b** is predicted to decrease as the reaction proceeds, even if the catalytic amount of charge carrier is maintained constant. Indeed the rate law in eq 16 indicates that under such conditions, the instantaneous first-order apparent rate constant $k^{ap} = k_{11}k_{10}[\mathbf{2b}^+]/[k_{11} + k_{-10}[\mathbf{2b}]]$ decreases when the conversion increases.

In the above discussion it was implicitely assumed that the concentration in the central chain propagating species, $[\mathbf{2b}^+]$, was constant. This is certainly a likely assumption under electrochemical conditions as in Figure 3, where $\mathbf{2b}^+$ is constantly regenerated at the electrode. Yet under homogeneous conditions, this supposes that the complete conversion is achieved within a time scale much smaller than any competitive consumption of the cationic species $\mathbf{2b}^+$. This is not the case, as evidenced by the incomplete conversion and the poor turnover numbers observed in Table I. In fact, from the voltammetric data in Figure 4, it is seen that the chemical stability of $\mathbf{2b}^+$ is not total within the time scale corresponding to the propagation of the chain conversion in Scheme III. Thus the chemical reaction in eq 13 acts as a termination step for the catalytic sequence, as shown in Scheme IV where steps a–c feature respectively the electron-transfer activation (eq 10), the

(19) (a) Loupy, A.; Tchoubar, B. *Effets de Sels en Chimie Organique et Organométallique*; Dunod Université: Paris, 1988. (b) Long, S. A.; Mc David, S. S.; *Chem. Rev.* **1952**, *51*, 119. (c) Gordon, J. E. *The Organic Chemistry of Electrolyte Solutions*; Wiley: New York, 1975. (d) Breslow, R.; Guo, T. *J. Am. Chem. Soc.* **1988**, *110*, 5613.

intramolecular ligand substitution (eq 11), and the termination step.

Thus, the amount of the propagating species, **2b**$^+$, decays in the homogeneous phase while the cycle propagates, which results in the failure of the latter to reach complete conversion under the homogeneous conditions in Table I. The exact kinetic effect of the deactivation step depends on its chemical nature and molecularity. Evidence for the latter is given by the electrochemical data obtained for **2b** oxidation in the presence of added phosphine (see Figure 5). Indeed the phosphine ligand does not react with **2b**$^+$ but with the product(s) of further evolution of the latter, to give the cation radical **4b**$^+$, as summarized in eq 19.

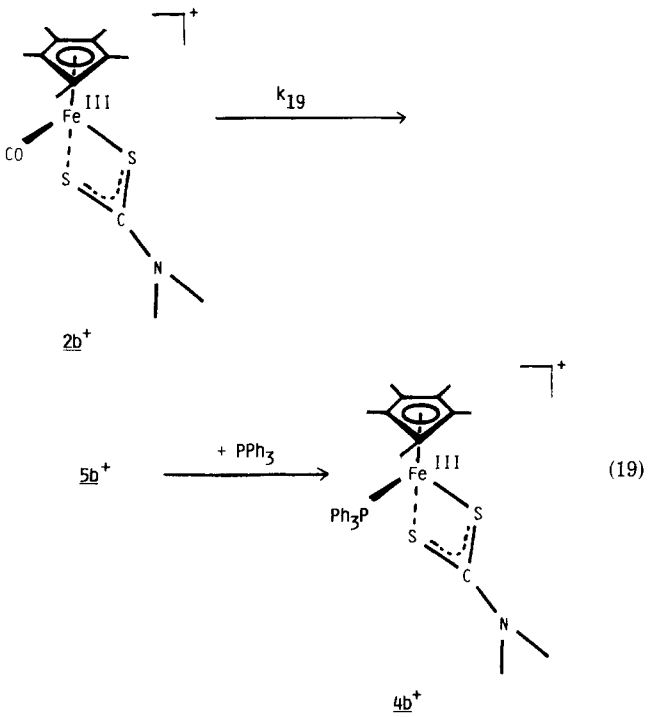


(19)

We now independently know that CO substitution by THF is fast even at −20 °C and proceeds according to an associative mechanism. This leads to the proposal that **5b**$^+$ is [FeCp*($\eta^2$-dtc)(THF)]$^+$. The process **2b**$^+$ → **5b**$^+$ is first order. Then, the kinetic sequence in Scheme IV corresponds to the exponential decay of **2b**$^+$ with time in eq 20, where $[\mathbf{2b}^+]_0$ is the initial concentration of **2b**$^+$, at the end of the induction period considered as the origin of time.

$$[\mathbf{2b}^+] = [\mathbf{2b}^+]_0 \exp(-k_{19}t) \qquad (20)$$

Introduction of this rate law into kinetic law 16, followed by integration, gives the conversion yield, $y_\infty$, at time infinite in eq 21.

$$\ln (1 - y_\infty) + y_\infty\left[\frac{k_{-10}[\mathbf{1b}]_0}{k_{11} + k_{-10}[\mathbf{1b}]_0}\right] = -\frac{[\mathbf{2b}^+]_0 k_{11} k_{10}}{[\mathbf{1b}]_0 k_{19} k_{-10}}\left[\frac{k_{-10}[\mathbf{1b}]_0}{k_{11} + k_{-10}[\mathbf{1b}]_0}\right] \qquad (21)$$

The variations of $y_\infty$ with the different parameters in eq 21 are represented in Figure 7. From the amount of reversibility of the $O_2/R_2$ wave in the voltammograms in Figure 4, one obtains $k_{19} \simeq 0.1$ s$^{-1}$. On the other hand, the term within brackets in eq 21 is estimated as close to 0.5 from the data obtained above. Thus, from eq 21, the experimental yields corresponding to the homogeneous experiments in Table I are predicted to be 36% and 45% for **1b** conversion (for $k_{11} = 10^7$ s$^{-1}$, $k_{11} = k_{-10}[\mathbf{1b}]_0$) for 0.1

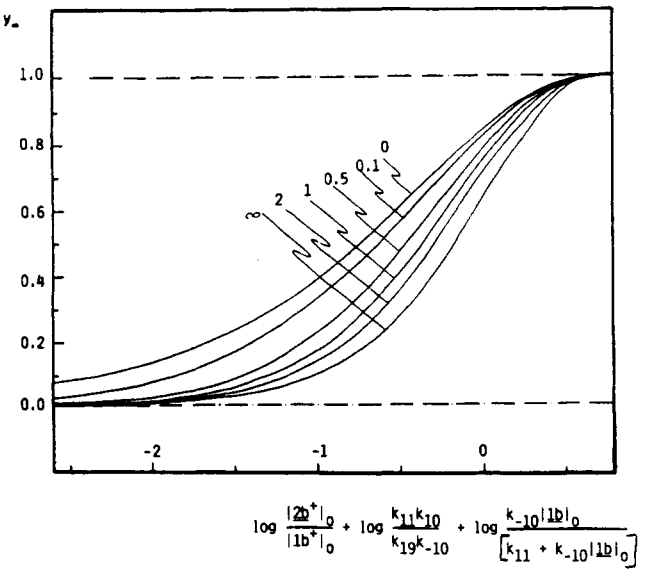


**Figure 7.** Variations of the conversion yield, $y_\infty$, at infinite time for the ETC sequence in Scheme IV, as given by eq 21 (see text). Numbers on the curves are values of $k_{11}/k_{-10}[\mathbf{1b}]_0$.

and 0.2 equiv of **3**, respectively, that compare with the experimental yields of 30% and 39% respectively obtained under the homogeneous conditions (presence of $[nBu_4N^+][BF_4^-]$ in THF; see part 2 in the Experimental Section).

**II. Oxidative Activation of Carbon Monoxide Substitution by Phosphine.** The cyclic voltammetries in Figure 5 demonstrate that carbon monoxide substitution occurs at the level of the intermediate species **5b**$^+$, in eq 19, which results from chemical substitution of CO by a THF ligand in the cationic complex **2b**$^+$. **5b**$^+$ gives rise to oxidation wave $O_3$ and reduction waves $R_3$ and $R_4$ in Figure 4. The latter waves are also observed in the reduction voltammogram of the phosphine-substituted cation **4b**$^+$$PF_6^-$, in the absence of free phosphine, and disappear when phosphine is added. Such behavior can be accounted for the combined sequence of reactions 22 and 23, which amounts to a catalytic conversion of **4b**$^+$ into **5b**$^+$ into the absence of phosphine.

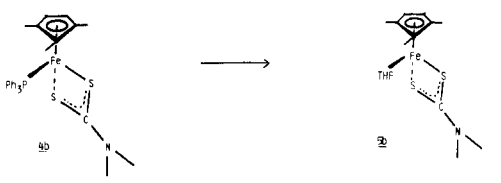

(22)

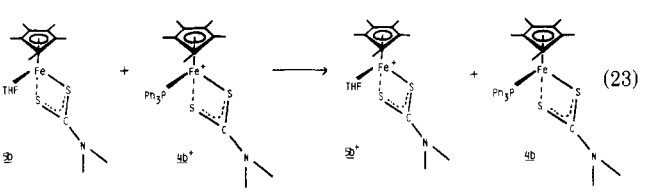

(23)

All the above observations indicate that **5b**$^+$ is a common intermediate formed either by carbon monoxide release from **2b**$^+$ or by phosphine expulsion from **4b**$^+$. They also confirm the results obtained chemically or by bulk electrosynthesis (vide supra): the coordination of a solvent (THF) molecule in **5b**$^+$ corresponding to the 17e structure [FeCp*($\eta^2$-dtc)(THF)]$^+$$PF_6^-$.

We now discuss the special feature of the carbon monoxide substitution in Scheme V, which occurs at the level of the oxidation wave $O_2$ of the chelated iron complex **2b**.

**Scheme V**

$$\mathbf{2b} - e^- \rightleftharpoons \mathbf{2b}^+ \quad (24)$$

$$\mathbf{2b}^+ \xrightarrow{k_{19}} \mathbf{5b}^+ + CO \quad (25)$$

$$\mathbf{5b}^+ + PPh_3 \xrightarrow{k_{27}} \mathbf{4b}^+ \quad (26)$$

**Scheme VI**

Part A

$$1b \xrightarrow{[FeCp_2^+]} 1b^+ + FeCp_2 \quad (27)$$

$$1b^+ \longrightarrow 2b^+ + CO \quad (28)$$

$$2b^+ + THF \longrightarrow 5b^+ + CO \quad (29)$$

$$5b^+ + PPh_3 \longrightarrow 4b^+ + THF \quad (30)$$

Part B

$$1b + [FeCp_2^+] \longrightarrow 1b^+ + FeCp_2 \quad (31)$$

$$1b^+ + PPh_3 \longrightarrow \underset{6b^+}{[Me_5C_5(OC)Fe(PPh_3)S{-}C(=S){-}NMe_2]^+} + CO \quad (32)$$

$$6b^+ \longrightarrow 4b^+ + CO \quad (33)$$

Indeed, for most of the reported ligand substitutions catalyzed via oxidative electron transfer, associative mechanisms are observed.[2,3]

In the last part of this section we discuss the mechanism of homogeneous carbon monoxide substitution by phosphine (eq 4) and dtc chelation in Scheme II. A priori, the two limiting paths in Scheme VI can be envisioned, according to the order of dtc chelation or of the phosphine ligation.

Thus Scheme VIA, which involves a combination of steps established independently (vide supra), is observed when chelation of the dtc ligand occurs at the level of $\mathbf{1b}^+$, whereas the sequence in Scheme VIB corresponds to a phosphine attack prior to the dtc chelation. On the other hand, one may suggest that CO loss occurs as the first step in the chemical evolution of $\mathbf{1b}^+$ (Scheme VII), since the latter is certainly less stabilized than $\mathbf{2b}^+$ (compare $k_{11} \simeq 10^7$ s$^{-1}$ to $k_{19} \simeq 0.1$ s$^{-1}$).

Yet, for the same reason, an associative mechanism such as those in reactions 35 and 36a,b is also reasonable. It is thus impossible to decide between the associative or dissociative nature of the carbon monoxide substitution at $\mathbf{1b}^+$ on such a basis. Yet, in both situations the dichotomy in Scheme VI is conditioned by the relative nucleophilicity of the chelating dithiocarbamate and of the phosphine ligands. Note that $[FeCp^*(CO)(NCMe)(PPh_3)]^+PF_6^-$ reacts with $Na(dtc)\cdot 2H_2O$ to give **2b** and $PPh_3$[16] (eq 37) and that the chelation of the dtc ligand in a neutral iron complex also proceeds with displacement of the triphenylphosphine (eq 38).

Such an effect should even be enhanced at the level of the cation radicals owing to the stabilization due to the dtc ligand. Thus, we are inclined to favor the sequence in Scheme VIA as a likely mechanism for $\mathbf{4b}^+$ formation from **1b**.

## Summary and Conclusion

The clean one-electron oxidant ferrocenium induces the ET-catalyzed chelation of **1a** and **1b** with low Coulombic

**Scheme VII**

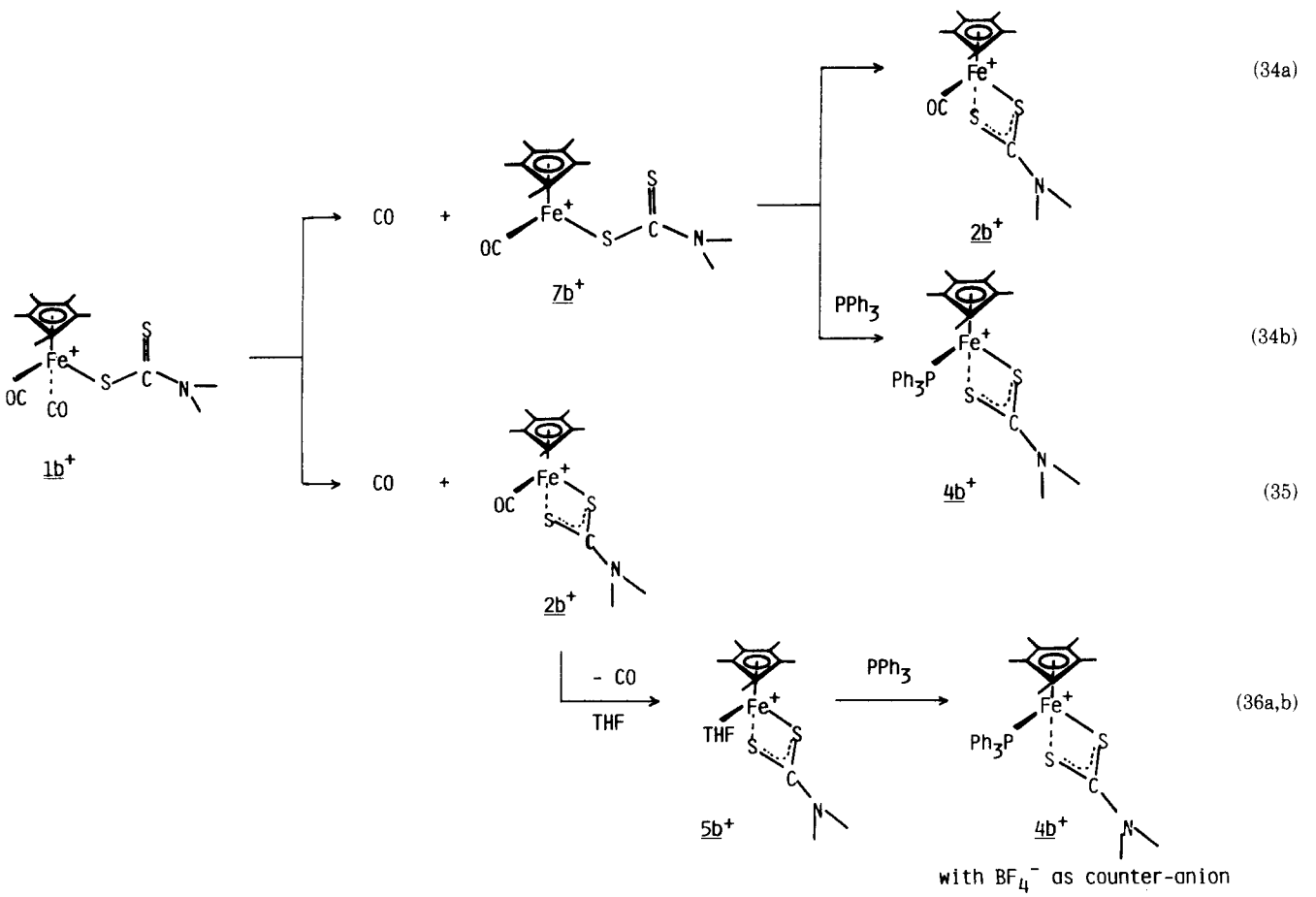

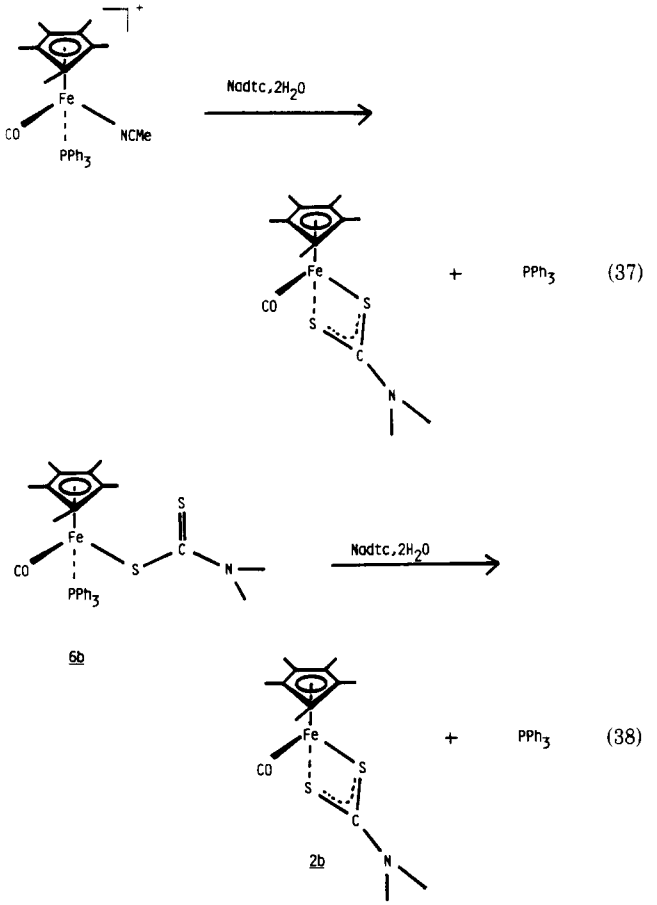


efficiencies due to the endergonicity of the cross-ET propagation step. Consequently side processes of $2^+X^-$ compete efficiently with the cross-ET step and break the propagation chain. In this context the counteranion of the ferrocenium salt plays a role in this competition since yields of **2b** are greater as the counteranion is larger. The nature of the side process of $2^+X^-$ depends on the nature of the medium since a large excess of electrolyte solubilizes $\mathbf{2b}^+X^-$, which provokes the CO substitution.

The facile electron-transfer catalysis of the intramolecular carbon monoxide substitution by chelation of the dithiocarbamate ligand in **1b** has been shown to proceed via the intermediacy of the cationic species $\mathbf{1b}^+X^-$ with a rate constant above $10^6$ $s^{-1}$. An efficient and rapid chain reaction thus ensues owing to the involvement of the electron transfer between the chelated cation $\mathbf{2b}^+X^-$ and reactant **1b**. In the absence of any termination step, such a chain process in Scheme III would convert all the starting material to its chelated form, **2b**, within a few seconds as observed in cyclic voltammetry (Figure 3) and in chemically induced reactions monitored under the same conditions. However, under the conditions of Table I, the partial precipitation ($\mathbf{2b}^+X^-$) or decomposition ($\mathbf{2a}^+X^-$), with a rate constant of 0.1 $s^{-1}$, acts as efficient termination steps that deactivate the above chain before completion of the conversion. Thus, the sequence in Scheme IV has been shown to account for the experimental conversion yields, as well as for the experimental conversion times.

In the presence of added phosphine and of stoichiometric quantities of ferrocenium as oxidant, the monodentate (dimethyldithiocarbamato)dicarbonyliron complex **1b** is efficiently converted to the chelated dtc monophosphine cation radical derivative $\mathbf{4b}^+X^-$. Although not rigorously established, we favor the intermediacy of the chelated (dimethyldithiocarbamato)carbonyliron cation radical $\mathbf{2b}^+$ in the process. This is supported by the observed facile carbon monoxide ligand substitution by phosphine through an associative mechanism and by the relative coordinating strength of the dtc and triphenylphosphine ligands.

Finally, we wish to mention the reversible phosphine decoordination occurring in the neutral dtc-chelated phosphine iron complex **4b**, which is additional evidence of the strong chelating abilities of the dithiocarbamato ligand.

## Experimental Section

**General Data.** Reagent grade tetrahydrofuran (THF), diethyl ether, and pentane were predried on Na foil and distilled from sodium benzophenone ketyl under argon just before use. Toluene was treated identically and stored under argon. Acetonitrile ($CH_3CN$) was stirred under argon overnight on phosphorus pentoxide, distilled from sodium carbonate, and stored under argon. Methylene chloride ($CH_2Cl_2$) was distilled from calcium hydride just before use. All other chemicals were used as received. All manipulations were done by Schlenk technique or in a nitrogen-filled Vacuum Atmosphere drylab. Infrared spectra were recorded with a Perkin-Elmer 1420 ratio recording infrared spectrophotometer that was calibrated with polystyrene. Samples were examined in solution (0.1-mm cells with NaCl windows), between NaCl disks in Nujol, or in KBr pellets. $^1H$ NMR spectra were recorded with a Brücker AC 200 (200 MHz) spectrometer. $^{13}C$ NMR spectra were obtained in the pulsed Fourier transform mode at 20.115 MHz with a Brücker WP 90 spectrometer and at 50.327 MHz with the same spectrometer. All chemical shifts are reported in parts per million ($\delta$) with reference to tetramethylsilane ($Me_4Si$) and were measured relative to the solvent or $Me_4Si$. ESR spectra were recorded by using a Brücker ER 200 ttX band. Cyclic voltammetry data were recorded with a homemade fast-scan potentiostat with positive feedback ohmic drop compensation, equipped with a PAR 175 waveform generator. Data were recorded on a 3091 Nicolet digital oscilloscope. Preparative electrolyses were performed with a Tacussel potentiostat and coulometric integrations with a Tacussel coulometer. All the potentials are given vs the SCE reference electrode equipped with a salt bridge (THF, $[nBu_4N^+][BF_4^-]$ 0.3 M) of composition identical with that of the investigated solution. The potential scale was calibrated vs ferrocene oxidation wave. Mössbauer spectra were recorded with a 25-mCi $^{57}Co$ source on Rh, using a symmetric triangular sweep mode. Elemental analyses were performed by the Center of Microanalyses of the CNRS (Lyon–Villeurbanne).

**Preparations.** The following abbreviations will be used for sake of clarity: $\eta^5\text{-}C_5H_5$ = Cp; $\eta^5\text{-}C_5(CH_3)_5$ = Cp*; dtc = $S_2CNMe_2$.

**1. Electrocatalytic Chelation of $[FeCp^*(\eta^1\text{-dtc})(CO)_2]$ (1b) by $[FeCp_2]^+PF_6^-$.** A 0.100-g sample of complex **1b** (0.2725 mmol) and 0.1 equiv of $[FeCp]_2^+PF_6^-$ (0.009 g, 0.0272 mmol) were closely mixed in the dark before addition of 5 mL of oxygen-free THF. The reaction time was fixed at 15 min because the ratio between **1b** and **2b** (given by IR spectroscopy) did not change after this period of time. THF was then removed in vacuo, and the crude product extracted in the dark with ether and filtered in another Schlenk tube. The solution was then evaporated in vacuo, and the porportion of both complexes was estimated both by $^1H$ NMR and infrared spectroscopies and correctly determined after separation.

This procedure was used for the chelation of $[Fe(\eta^5\text{-}C_5R_5)(\eta^1\text{-dtc})(CO)_2]$ (R = H, Me) by $x$ equiv of $[FeCp_2]^+X^-$ ($x$ = 0.05, 0.07, 0.1, 0.15, 0.2, 0.3, 0.4, 0.5, 1.0, $X^-$ = $PF_6^-$; and $x$ = 0.1, X = $BF_4^-$, $PF_6^-$, $SbCl_6^-$): see Tables I and II for results. For $x$ = 1 equiv of $[FeCp_2]^+PF_6^-$, a green precipitate formed that was analyzed as $[FeCp^*(\eta^2\text{-dtc})(CO)]^+PF_6^-$ by comparison with an authentic sample.[16]

**2. Electrocatalytic Chelation of $[FeCp^*(\eta^1\text{-dtc})(CO)_2]$ (1b) by $[FeCp_2]^+BF_4^-$.** A 0.100-g sample of complex **1b** (0.2725 mmol), $x$ equiv of $[FeCp_2]^+BF_4^-$ ($x$ = 0.1, 0.2), and 10 equiv of $[nBu_4N^+][BF_4^-]$ (0.900 g, 2.725 mmol) were closely mixed in the dark before addition of 5 mL of oxygen-free THF. The reaction time was fixed at 15 min for the same reasons as in 1. The same workup as in 1 gave 30% of **2b** for $x$ = 0.1 and 39% of **2b** for $x$ = 0.2.

**3. Electrocatalytic Chelation of $[FeCp^*(\eta^1\text{-dtc})(CO)_2]$ by 0.1 Equiv of $[FeCp_2]^+PF_6^-$ in $CH_2Cl_2$.** A 0.1-g sample of complex **1b** (0.2725 mmol) and 9 mg of $[FeCp_2]^+PF_6^-$ were stirred in $CH_2Cl_2$ in the dark, under argon for 10 min. The solvent was then evaporated, and the crude product extracted with dry ether, which was then evaporated. The same workup as in 1 gave 12% yield for complex **2b** and 68% yield for the starting material **1b**.

**4. Chelation of $[FeCp^*(\eta^1\text{-dtc})(CO)_2]$ by 1 Equiv of $[FeCp_2]^+BF_4^-$ in the Presence of $[nBu_4N^+][BF_4^-]$.** A 0.054-g sample of complex **1b** (0.147 mmol), 0.040 g of $[FeCp_2]^+BF_4^-$ (0.147 mmol), and 2 g of $[nBu_4N^+][BF_4^-]$ (6.079 mmol) were stirred at room temperature, in the dark, under argon in 10 mL of THF for 10 min. A red-brown color immediately appeared. Evaporation of the solvent gave an orange-brown powder that showed the same ESR spectrum as the product obtained by electrosynthesis, indicating the structure $[FeCp^*(\eta^2\text{-dtc})(THF)]^+BF_4^-$ (ESR (solid-state sample, 10 K) $g_1 = 2.323$, $g_2 = 2.050$, $g_3 = 2.004$).

**5. $[FeCp^*(\eta^2\text{-dtc})(PPh_3)]^+PF_6^-$ ($4b^+PF_6^-$).** A 0.300-g sample of complex **1b** (0.817 mmol) in 10 mL of $CH_3COCH_3$ was stirred with 0.214 g (0.817 mmol) of triphenylphosphine and 0.270 g (0.817 mmol) of $[FeCp_2]^+PF_6^-$ for 30 min at room temperature under argon. The red-purple solution was then filtered through a Celite column (1-cm height) and washed with $CH_3CN$. Addition of absolute ethanol was followed by a recrystallization by slow evaporation of $CH_3CN$ without warming. Purple microcrystalline powder of complex $4b^+PF_6^-$ (0.507 g, 86% yield) was recovered and identified by comparison with an authentic sample.

**6. Bulk Electrolysis of 1b.** Electrochemical 1e oxidation of 0.369 g of **1b** (1 mmol) was performed in 30 mL of THF-0.3 M $[nBu_4N^+][BF_4^-]$, in a divided cell. The anodic compartment was equipped with a gold grid (5 $cm^2$) as the working electrode and a SCE + THF, 0.3 M $[nBu_4N^+][BF_4^-]$ salt bridge as the reference electrode. The cathodic reaction was reduction of 4-chlorobenzonitrile at a platinum gauze electrode (5 $cm^2$). Oxidation was performed at 1 V vs SCE. After 1 F/mol was passed, cyclic voltammetry showed that 99% of the starting material had disappeared, to lead to the observation of the CV traces observed in microelectrolytic conditions in Figure 4. The homogeneous red-brown solution thus obtained was pumped off to dryness, to afford a solid residue (90% $[nBu_4N^+][BF_4^-]$, 10% of electrolysis product, which was characterized by comparison with an authentic sample).

**Acknowledgment.** Helpful experimental assistance by N. Ardoin (Université de Bordeaux I) and early work by D. Catheline (Université de Rennes I) are gratefully acknowledged. We thank the "Région Aquitaine", the CNRS (URA 35, 110, and 415), the "Université de Bordeaux I", and the "Ecole Normale Supérieure" for financial support.

**Registry No.** **1a**, 75900-10-6; **1b**, 89875-07-0; **2a**, 12128-65-3; **2b**, 84541-24-2; $2b^+PF_6^-$, 119366-46-0; **3a**, 11077-24-0; **3b**, 1282-37-7; **3c**, 98092-06-9; $4b^+PF_6^-$, 118228-79-8; $5b^+BF_4^-$, 124945-07-9.

# (Dithiocarbamato)iron(II) Complexes: Photochemical Chelation and Ligand Exchange, Comparison with Electron-Transfer Processes, and X-ray Crystal Structures of $Fe(\eta^5\text{-}C_5Me_5)(\eta^1\text{-}SC(S)NMe_2)(CO)_2$ and $Fe(\eta^5\text{-}C_5Me_5)(\eta^2\text{-}S_2CNMe_2)(PPh_3)$

Marie-Hélène Desbois,[†] Christine M. Nunn,[‡] Alan H. Cowley,*[,‡] and Didier Astruc*[,†]

*Laboratoire de Chimie Organique et Organométallique, UA CNRS No. 35, Université de Bordeaux I, 351, Cours de la Libération, 33405 Talence Cédex, France, and Department of Chemistry, College of Natural Sciences, The University of Texas, Austin, Texas 78712-1167*

*Received June 15, 1989*

The X-ray crystal structure of $FeCp^*(\eta^1\text{-dtc})(CO)_2$ (**1**, $Cp^* = \eta^5\text{-}C_5Me_5$, $dtc = S_2CNMe_2$) confirms that the dithiocarbamate ligand is bound to iron in a monodentate mode. The photochemical chelation of **1** is carried out in dichloromethane using visible light and quantitatively gives the chelate $FeCp^*(\eta^2\text{-dtc})(CO)$ (**2**) and CO. This reaction is the best route to **2** and compares with the electron-transfer chain (ETC) processes **1** → **2** catalyzed by either oxidizing or reducing agents. The photolytic reaction, which can be carried out by monochromatic (330 nm) irradiation and monitored by visible spectroscopy, gives two isosbestic points at 394 and 432 nm. The quantum yield ($\Phi \simeq 0.6$) does not vary greatly with the polarity of the solvents, which indicates that this process is stoichiometric:photolysis of **2** in ether in the presence of **1** equiv of $PPh_3$ using visible light gives $FeCp^*(\eta^2\text{-dtc})(PPh_3)$ (**3**) in 80% yield and CO. This reaction compares with the stoichiometric one-electron oxidation of **1** or **2** giving $3^+$ in the presence of $PPh_3$, followed by the one-electron reduction of $3^+$ to **3**. Both complexes **1** and **3** crystallize in a triclinic system. **1**: $a = 8.582$ (2) Å, $b = 9.046$ (4) Å, $c = 12.377$ (7) Å, $\alpha = 97.05$ (4)°, $\beta = 96.84$ (3)°, $\gamma = 111.99$ (3)°, space group $P\bar{1}$, $Z = 2$, $V = 869.9$ Å$^3$, $\rho_{calcd} = 1.40$ g/cm$^3$, $R = 0.058$, $R_w = 0.091$ based on 3232 reflections with $F_o > 3\sigma(F_o)$. **3**: $a = 11.142$ (4) Å, $b = 14.958$ (4) Å, $c = 10.382$ (4) Å, $\alpha = 98.22$ (2)°, $\beta = 115.22$ (3)°, $\gamma = 102.62$ (3)°, space group $P\bar{1}$, $Z = 2$, $V = 1471.9$ Å$^3$, $\rho_{calcd} = 1.29$ g/cm$^3$, $R = 0.056$, $R_w = 0.070$ based on 4315 reflections with $F_o > 3\sigma(F_o)$. The X-ray crystal structure of **3** shows the bulk around iron, responsible for the stability of the radical $3^+$.

## Introduction

Inorganic dithiocarbamate (dtc) complexes are well-known,[1] but complexes containing both a dithiocarbamate and a Cp* ligand offer the opportunity of studying mixed inorganic-organometallic behavior. For instance, the chelation of $FeCp^*(\eta^1\text{-dtc})(CO)_2$ (**1**)[2] to $FeCp^*(\eta^2\text{-dtc})(CO)$ (**2**, eq 1) is the first reaction shown to be electrocatalyzed

[†] Université de Bordeaux I.
[‡] The University of Texas.

(1) (a) Fackler, J. P. *Adv. Chem. Ser.* **1976**, *150*, 394. (b) Thorn, G. D.; Ludwig, R. A. *The Dithiocarbamates and Related Compounds*; Elsevier: Amsterdam, 1962. (c) Livingstone, S. E. *Q. Rev. Chem. Soc.* **1965**, *19*, 416. (d) Eisenberg, R. *Prog. Inorg. Chem.* **1970**, *12*, 295. (e) Coucouvanis, D. *Prog. Inorg. Chem.* **1970**, *11*, 233. (f) Willemse, J.; Gras, J. A.; Steggarda, J. J.; Kiegzers, C. P. *Struct. Bonding (Berlin)* **1976**, *28*, 83.

0276-7333/90/2309-0640$02.50/0 